Strong Indian Ocean sea surface temperature signals associated with the Madden-Julian Oscillation in late 2007 and early 2008

J. Vialard,[1] G. R. Foltz,[2] M. J. McPhaden,[3] J. P. Duvel,[4] and C. de Boyer Montégut[5]

Received 8 July 2008; accepted 3 September 2008; published 15 October 2008.

[1] A moored buoy was recently deployed at 8°S, 67°E in the shallow thermocline region of the Indian Ocean known as ''Seychelles-Chagos Thermocline Ridge'' (SCTR), where the Madden Julian Oscillation (MJO) is associated with strong sea surface temperature (SST) variability. We use observations from this mooring to describe the oceanic signature of two MJOs between November 2007 and February 2008. The four-month average upper ocean heat balance was largely between heating by atmospheric forcing (2.0 ± 0.3°C/month) and a significant cooling by subsurface processes (-2.2 ± 0.8°C/month), consistent with climatological Ekman pumping in the region. The two MJO events resulted in strong intraseasonal SST variations (1.5 to 2°C in ~20 days) in the SCTR. At the mooring site, atmospheric fluxes dominated the upper ocean heat balance at the MJO timescale, with the net surface heat flux into the ocean decreasing from an average 105 W m^{-2} during suppressed phases to 15 W m^{-2} during active phases of the MJO. It is difficult to establish if MJO-induced variations of subsurface processes also contributed to the cooling because of large uncertainty in this term. Lateral advection had no systematic fluctuations on MJO timescales, but cannot be neglected at the mooring site. **Citation:** Vialard, J., G. R. Foltz, M. J. McPhaden, J. P. Duvel, and C. de Boyer Montégut (2008), Strong Indian Ocean sea surface temperature signals associated with the Madden-Julian Oscillation in late 2007 and early 2008, *Geophys. Res. Lett.*, *35*, L19608, doi:10.1029/2008GL035238.

1. Introduction

[2] The Madden-Julian Oscillation (MJO) is a large-scale dynamical and convective intraseasonal perturbation of the tropical troposphere (see *Zhang* [2005] for a review), with a clear signature in sea surface temperature (hereafter, SST) [e.g., *Hendon and Glick*, 1997; *Shinoda and Hendon*, 1998]. Modeling studies suggest that considering the coupling between the atmosphere and the ocean can improve simulations [e.g., *Maloney and Sobel*, 2004] and forecasts [*Woolnough et al.*, 2007] of the MJO.

[1] Laboratoire d'Océanographie Expérimentation et Approches Numériques, IRD, Paris, France.
[2] Joint Institute for the Study of the Atmosphere and Ocean, University of Washington, Seattle, Washington, USA.
[3] Pacific Marine Environment Laboratory, NOAA, Seattle, Washington, USA.
[4] Laboratoire de Météorologie Dynamique, CNRS, Paris, France.
[5] Frontier Research Center for Global Change, JAMSTEC, Yokohama, Japan.

0094-8276/08/2008GL035238

[3] Earlier studies [e.g., *Hendon and Glick*, 1997; *Shinoda and Hendon*, 1998] suggested that surface flux perturbations drive the MJO SST signal. These studies used satellite measurements of SST in the infrared window, for which the screening effect of clouds prevents an accurate estimate of ocean cooling below convective systems [*Duvel and Vialard*, 2007]. The use of microwave instruments, like the Tropical Rainfall Measuring Mission Microwave Instrument [*Wentz et al.*, 2000], revealed two previously unnoticed regions of strong intraseasonal variability of the SST during boreal winter: the Indian Ocean between 5°S and 10°S and seas located north of the Australian continent [*Saji et al.*, 2006; *Duvel and Vialard*, 2007]. The first of these regions is located over the ''Seychelles-Chagos Thermocline ridge'' (hereafter SCTR) induced by climatological Ekman pumping. *Duvel et al.* [2004] suggested that a shallow thermocline in this region contributes to the strong SST variability by maintaining a shallow and more responsive mixed layer. They suggested that surface heat fluxes dominate the heat budget based on a case study of two strong cooling events in 1999. Investigating the same events, *Harrison and Vecchi* [2001] proposed that enhanced Ekman pumping due to MJO forcing was responsible for the cooling. In situ measurements are thus needed to provide an improved description of the oceanic signature of the MJO in this region.

[4] A moored buoy was deployed at 8°S, 67°E in January 2007 during the Cirene cruise [*Vialard et al.*, 2008], within the framework of the Research Moored Array for African-Asian-Australian Monsoon Analysis and Prediction program (RAMA) [*McPhaden et al.*, 2008]. This mooring has now provided more than one year of surface meteorological and subsurface data. In this paper, we use these data to document the surface flux perturbations and upper ocean MJO signature in this region. In section 2, the datasets and simple heat budget computation are described. In section 3, we use satellite data to describe the large-scale signature of the MJO during November 2007–February 2008. Section 4 describes the oceanic signals and surface layer heat budget at 8°S, 67°E. We conclude with a brief discussion in section 5.

2. Data

[5] The NOAA interpolated outgoing longwave radiation (OLR) [*Liebmann and Smith*, 1996] is used to detect regions of atmospheric deep convection. Optimally interpolated SST combining TMI (on TRMM) and AMSR-E (on AQUA) microwave instrument and surface wind data from

QuickScat scatterometer are also used. Both datasets are available on a regular 0.25° grid and we used daily data for SST and 3-day sliding averages for wind.

[6] A next generation Autonomous Temperature Line Acquisition System (ATLAS) mooring supplied by NOAA's Pacific Marine Environmental Laboratory (PMEL) was deployed at 8°S, 67°E in January 2007. Measurements, continued through the present, include subsurface temperature and salinity, air temperature, relative humidity, wind velocity, shortwave radiation, and precipitation. Ocean temperature is measured at 1, 5, 10, 20, 40, 60, 80, 100, 120, 140, 180, 300 and 500 m. Salinity is measured at 1 m, 10 m, 20 m, 40 m, 60 m, 100 m and 140 m. SST and SSS are given by measurements taken at 1 m. Oceanic currents are measured at 10 m. Meteorological measurements are made 3–4 m above sea level. We use daily averaged data for the time period November 2007–February 2008.

[7] We consider a simplified version of the mixed layer (ML) heat balance. A brief description of the computation of the heat balance follows, completed by a more detailed explanation and description of the error bars available as auxiliary material.[1]

$$\frac{\partial T}{\partial t} = \frac{Q_0}{\rho c_p h} - u\frac{\partial T}{\partial x} - v\frac{\partial T}{\partial y} + R \qquad (1)$$

Here h is the ML depth (MLD), ρc_p the volumic heat capacity of seawater, T the average ML temperature and u,v the mixed layer currents. The left hand side of (1) is the ML temperature change rate, estimated from the mooring subsurface data. Q_0, the surface heat flux corrected for the penetration of shortwave radiation through the base of the ML, is also estimated from the mooring measurements (see below). We computed horizontal advection using the observed currents at 10 m and TMI-AMSR-E SST gradients. R is the residual, accounting for exchanges with the subsurface (upwelling, entrainment and vertical turbulent heat flux at the base of the ML) and errors in the estimation of other terms in (1).

[8] We estimate h as the depth at which the density is 0.15 kg m^{-3} greater than density at 5 m. The salinity and temperature sensors at 20 m failed prior to the time period we consider, and the salinity sensor at 40 m failed in mid January. The limited vertical resolution, due to sensor failures, translates into a large uncertainty on the MLD. Since the MLD is a critical parameter for this study, we followed a two-step approach to improve its estimate, using a combination of historical data and an optimal interpolation using neighboring Argo profiles (see auxiliary material).

[9] Latent and sensible heat fluxes are estimated from the Coupled Ocean-Atmosphere Response Experiment (COARE) bulk flux algorithm version 3.0 [*Fairall et al.*, 2003] using the mooring SST, air temperature, relative humidity, and wind speed. Net surface shortwave radiation (SWR) is obtained from the downward shortwave flux measured by the mooring, assuming an albedo of 6%. The amount of SWR that penetrates below the ML is estimated following *Sweeney et al.* [2005], using monthly climatological SeaWiFS chlorophyll concentration. Net longwave radiation is estimated following the methodology of *Foltz and McPhaden* [2005]. We use the convention that surface heat fluxes are positive when they tend to heat the ML.

3. Large Scale Perturbations

[10] In late 2007 and early 2008, three large-scale convective episodes developed, with suppressed convective phases in between (Figure 1). The *Wheeler and Hendon* [2004] MJO index (not shown) is consistent with these active and suppressed convective phases. The three convective episodes propagate eastward at speeds between 2 and 6 m s^{-1} (the average speed for the MJO is 5 m s^{-1} [*Zhang*, 2005]). The first convective episode is confined to the western Pacific. A convectively active phase (A1) develops in December over the Indian Ocean, following the suppressed phase (S1), and propagates over the western Pacific until the end of January. The last active phase (A2) develops over the Indian Ocean in late January following the suppressed phase (S2), and remains over the maritime continent region in February.

[11] The associated SST perturbations tend to be strongest to the west of the convective anomaly (Figure 1c). This is the consequence of the delayed response of the ocean to atmospheric forcing and the fact that the wind perturbation is strongest to the west of the convective anomaly (Figure 1) [*Duvel and Vialard*, 2007]. The SST perturbation is strongest north and west of Australia, with anomalies up to ±2°C (Figure 2), and in the 0–10°S band in the Indian Ocean, with anomalies up to ±1.5°C. In mid-December (Figure 2a), A1 is associated with a large scale cooling (0.5 to 2°C amplitude) of the Indian Ocean between the equator and 10°S, while the maritime continent region is warm, due to S1. By early January (Figure 2b), the cooling associated with A1 has moved to the eastern Indian Ocean and maritime continent region, while the western Pacific experiences a moderate warming associated with S1. In mid January (Figure 2c), the surrounding of Australia is experiencing a ∼2°C intraseasonal cold anomaly, while the 0–10°S band in the Indian Ocean is anomalously warm (up to 1.5°C) during S2. In early February, in association with S2, the ocean surrounding Australia has warmed (up to 2°C anomaly), while the Indian Ocean cools during A2.

4. In Situ Measurements at 8°S, 67°E

[12] The ATLAS mooring at 8°S, 67°E is located in a region of strong MJO SST signal during late 2007 and early 2008. Buoy measurements between November 2007 and February 2008 are reported on Figure 3. The average values given in brackets below are computed over the warming/cooling periods highlighted in Figure 3. In November, during S1, easterlies are still relatively strong at the mooring (Figure 3a) and have not shifted yet to the weaker westerly regime generally observed from December to March at that location. This results in a relatively strong latent heat flux ∼−100 W m^{-2} (Figure 3b). However, downward shortwave flux is high (∼250 W m^{-2}) and there is sporadic rain (73 mm of accumulated rainfall), consistent with the influence of S1. From late November to mid December, westerly winds develop with speeds up to 8 m s^{-1}. More rain (187 mm of accumulated rainfall), reduced downward shortwave

[1] Auxiliary materials are available in the HTML. doi:10.1029/2008GL035238.

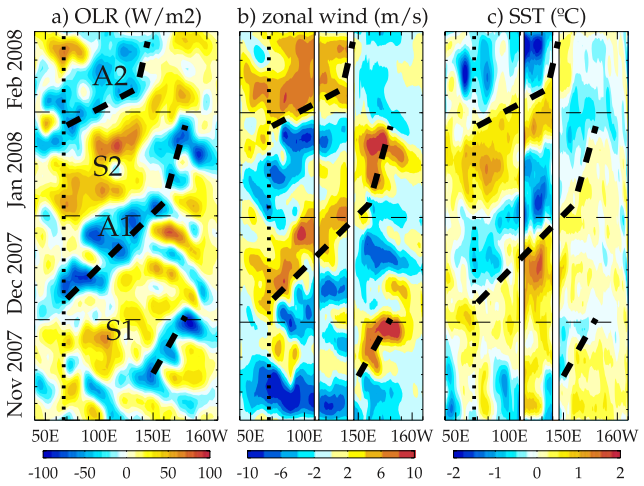

Figure 1. Time-section along 8°S: (a) NOAA OLR (W m^{-2}), (b) Quikscat surface zonal wind (m s^{-1}) and (c) TMI+AMSR-E SST (°C). A 10–90 day bandpass filter and 5° smoothing has been applied. The thick dashed lines highlight roughly the eastern edge of the deep convection at 8°S. The dotted line indicates the longitude of the mooring. The suppressed and active phases of atmospheric deep convection S1, A1, S2 and A2 (see text) have been labeled on Figure 1a.

radiation (192 W m^{-2}), and relatively strong latent heat flux (−100 W m^{-2}) are observed under the influence of A1. The net surface heat flux however remains positive (32 W m^{-2}). From mid December to early January, the suppressed phase S2 is associated with lighter winds (3.3 m s^{-1}), high downward shortwave radiation (244 W m^{-2}), reduced latent heat flux (−76 W m^{-2}), and more flux into the ocean (97 W m^{-2}). Rainfall is still significant (194 mm of accumulated rainfall), due to some remaining convective activity after A1. The A2 active phase has the most dramatic impact with strongly reduced downward shortwave radiation (150 W m^{-2}) and heavy rain (accumulated rainfall of 374 mm), increased latent heat loss (−106 W m^{-2}) due to stronger winds (6.1 m s^{-1}). Surface net heat flux becomes negative on average during A2 (−12 W m^{-2}).

[13] The ocean perturbation associated with the MJO is very clear from the buoy data (Figures 3c and 3d). The surface warming associated with the suppressed phases is of 1°C for S1 and of 1.6°C for S2. The surface cooling associated with the active phases is of 1°C for A1 and of 1.7°C for A2. In general there is a freshening after rainfall, but the clearest salinity signal is a sharp freshening of about 0.8 psu after the strong rain during A2. The MLD is between 20 and 30 m during S1. It becomes shallower during A1 (between 15 and 20 m) and S2 (between 10 and 15 m). The only significant deepening is observed during A2, with an average MLD of 30 m. The MLD variations cannot be explained entirely by surface heat flux variation associated with the MJO: for example the MLD is deeper during S1 than during A1, despite weaker winds and more upper ocean heat gain. Also, the MLD does not deepen significantly during A1 while it does during A2. In both cases, subsurface stratification –partly controlled by remote forcing– seem to also play a role in controlling the MLD, but this will be addressed in a separate study.

[14] The ML heat budget and its estimated errors are shown in Figure 3e. The 4 month average balance (see Table S1 of auxiliary material) is primarily between heating by atmospheric fluxes (2.0 ± 0.3°C $month^{-1}$) and cooling by vertical exchanges with the thermocline (turbulent and advective, −2.2 ± 0.8°C $month^{-1}$). The significant cooling by vertical processes is consistent with the notion of an upwelling driven by climatological Ekman pumping in the SCTR region.

[15] The surface heat flux term decreases strongly during the two active MJO periods, and is strong and positive during the suppressed phases. The surface flux term has a 0.89 correlation with the heat storage and comparable amplitude (standard deviation of 1.6°C $month^{-1}$ vs. 1.7°C $month^{-1}$ for the storage), indicative that surface fluxes are dominating the balance at the MJO timescale during that period.

[16] The mean cooling by vertical processes explains why SST decreases during MJO active phases even when the net heat flux remains positive (e.g., during most of A1). Previous studies suggested that *intraseasonal variations* of the Ekman pumping and vertical processes could also play a significant role in this region [*Harrison and Vecchi*, 2001; *Saji et al.*, 2006]. However, the residual is poorly correlated with the heat storage (0.29) and has a smaller standard

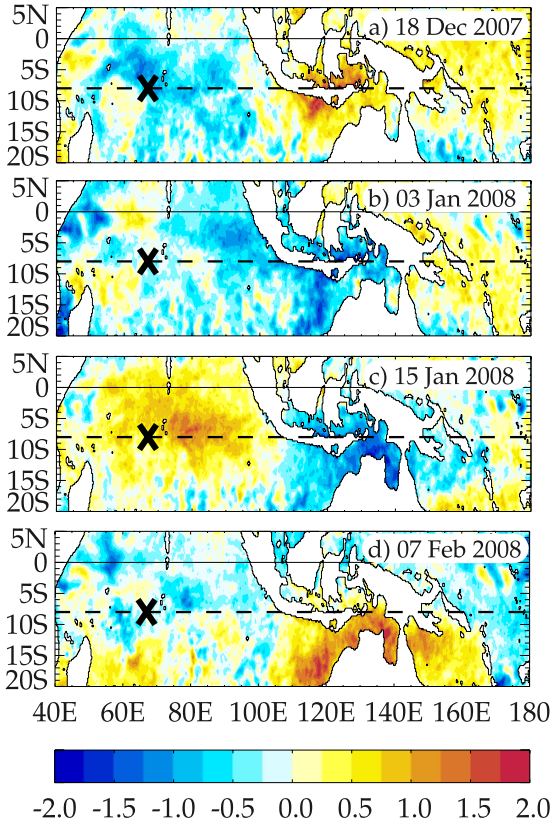

Figure 2. One-day snapshots of 10–90 day filtered TMI+AMSR-E SST (°C) on (a) 18 December 2007, (b) 3 January 2008, (c) 15 January 2008 and (d) 07 February 2008. These dates have been selected to highlight the various phases of the MJO SST signature during November 2007–February 2008. The dashed line indicates 8°S and the cross indicates the position of the ATLAS mooring.

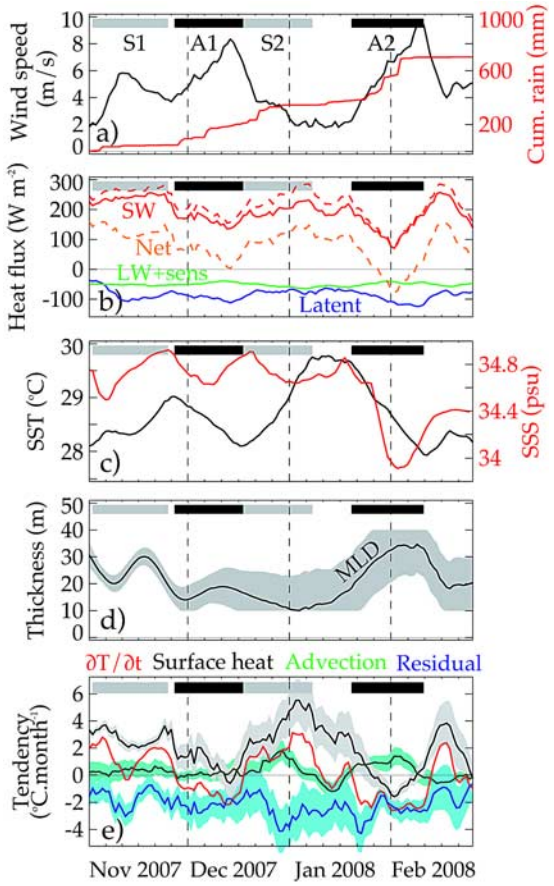

Figure 3. November 2007–February 2008 time series from the ATLAS mooring at 8°S, 67°E. (a) Wind speed (m s^{-1}, black) and accumulated TRMM rainfall (mm, red); (b) surface heat fluxes (W m^{-2}): surface shortwave flux (net: red dashed; absorbed by the mixed layer: red), latent heat flux (blue), sensible + longwave flux (green) and net heat flux (dashed orange); (c) SST (°C, black) and SSS (psu, red); (d) mixed layer depth (m) with one standard-deviation error bar (shading); and (e) mixed layer heat budget in °C $month^{-1}$ as in equation (1): mixed layer temperature tendency (red), atmospheric forcing heating rate (black), horizontal advection (green) and residual (blue), with shading indicating the one standard-deviation error bar. The error bar for the storage term is small and has not been plotted. All time series have been smoothed using a 7-day sliding average. The grey (black) overbars indicate warming (cooling) periods corresponding to suppressed (active) convection that are used to indicate average values in the text.

deviation (0.8°C $month^{-1}$ vs. 1.7°C $month^{-1}$ for the storage), suggesting that this is not the case. The 95% confidence interval for the suppressed minus active phase is 1.8 to 3.6 °C $month^{-1}$ for the flux and −0.7 to 1.4°C $month^{-1}$ for the residual. This shows that the atmospheric heat fluxes contributed more, but does not exclude a significant contribution from vertical processes on MJO timescales.

[17] The advection term is uncorrelated with the heat storage and has much smaller standard deviation (0.6°C $month^{-1}$ vs. 1.7°C $month^{-1}$ for the storage). Whereas advection is not negligible at the mooring site, it does not fluctuate systematically on MJO time scales (there is, for example, an advective warming of similar amplitude during both S2 and A2).

5. Discussion

[18] This study is consistent with previous work suggesting that atmospheric flux perturbations related to the MJO are the primary driver of the SST signatures on intraseasonal time scales in the southwestern Indian Ocean. At the mooring location, the shortwave flux was the biggest contributor, with a change of 84 W m^{-2} between active and suppressed phases vs. 18 W m^{-2} for the sensible plus latent heat flux. The effect of subsurface processes (entrainment, Ekman pumping) is smaller than surface fluxes, but the large uncertainty in this term does not preclude a significant increase of the cooling during MJO active phases as proposed by [*Harrison and Vecchi*, 2001; *Saji et al.*, 2006]. Horizontal advection does not seem to fluctuate in a systematic way at the time scales of the MJO, but it is not negligible at the mooring site. The results of this local study might not be applicable everywhere in the SCTR region. In particular, the relative weight of the various physical processes responsible for the SST perturbations may vary strongly between 10°S and the Equator [*Duvel et al.*, 2004]. The development of the RAMA array will hopefully allow for a more accurate and basin-scale view of the causes of the MJO SST signal in the future.

[19] Vertical processes cool the surface by an average -2.2 ± 0.8°C $month^{-1}$ over the duration of the study. The period over which this heat budget has been computed is quite short and the heat budget in this region will have to be estimated over a longer period. This value is however comparable to the -1.6 ± 0.3°C $month^{-1}$ value diagnosed in the Pacific equatorial upwelling region at 140°W by *Wang and McPhaden* [1999]. This result is consistent with the idea that the SCTR region is influenced by significant upwelling because of Ekman-pumping driven by the northward decrease of the southeast trades. One interesting question is how this region can sustain such a high SST (above 29°C in austral summer, compared to roughly 26°C at 140°W in the Pacific equatorial upwelling) in presence of upwelling, i.e., what allows the net heat flux to remain so strong in presence of such warm SST.

[20] The climatological upwelling mentioned above might be important to explain the large MJO SST signals observed in the SCTR region, by maintaining a shallow thermocline. *Duvel et al.* [2004] suggested that this shallow thermocline prevents the ML from excessively deepening during wind bursts, thus making it more reactive to air-sea flux intraseasonal variations. The uncertainty in MLD values, because of sensor failures, unfortunately does not allow us to confidently test this hypothesis. This issue will have to be addressed in future studies in which MLD is more accurately defined from higher vertical resolution data. It will also be interesting to investigate how interannual variability in SCTR thermocline depth can influence not only the amplitude of SST perturbations but also large-scale organized convective perturbations during MJO onset, as suggested by *Duvel and Vialard* [2007] and *Vialard et al.* [2008].

[21] We used daily mean surface fluxes and subsurface data in this paper. During suppressed phases of the MJO, heating is concentrated near the surface during the day, resulting in increased daily average SST. On the other hand, the formation of diurnal warm layers is prevented by stronger wind during suppressed phases. Several studies [e.g., *Shinoda and Hendon*, 1998] have shown that diurnal variability modulates SST intraseasonal variability as a result. It may be possible to quantify this potentially important effect upon recovery of the mooring, which will provide access to the 1- to 10-minute resolution internally recorded datasets.

[22] **Acknowledgments.** The lead author made his contributions to this paper while visiting the National Institute of Oceanography in Goa, India. QuikScat and Microwave OI SST data are produced by Remote Sensing Systems. Data are available at www.remss.com. GF and MJM thank NOAA's Climate Program Office for supporting this research. This is PMEL publication number 3198 and JISAO publication number 1488.

References

Duvel, J. P., and J. Vialard (2007), Indo-Pacific sea surface temperature perturbations associated with intraseasonal oscillations of the tropical convection, *J. Clim.*, *20*, 3056–3082.

Duvel, J. P., R. Roca, and J. Vialard (2004), Ocean mixed layer temperature variations induced by intraseasonal convective perturbations over the Indian Ocean, *J. Atmos. Sci.*, *61*, 1004–1023.

Fairall, C. W., E. F. Bradley, J. E. Hare, A. A. Grachev, and J. B. Edson (2003), Bulk parameterization of air-sea fluxes: Updates and verification for the COARE algorithm, *J. Clim.*, *16*, 571–591.

Foltz, G. R., and M. J. McPhaden (2005), Mixed layer heat balance on intraseasonal time scales in the northwestern tropical Atlantic Ocean, *J. Clim.*, *18*, 4168–4184.

Harrison, D. E., and G. A. Vecchi (2001), January 1999 Indian Ocean cooling event, *Geophys. Res. Lett.*, *28*, 3717–3720.

Hendon, H. H., and J. Glick (1997), Intraseasonal air-sea interactions in the tropical Indian and Pacific oceans, *J. Clim.*, *10*, 647–661.

Liebmann, B., and C. A. Smith (1996), Description of a complete (interpolated) outgoing longwave radiation dataset, *Bull. Am. Meteorol. Soc.*, *77*, 1275–1277.

Maloney, E. D., and A. H. Sobel (2004), Surface fluxes and ocean coupling in the tropical intraseasonal oscillation, *J. Clim.*, *17*, 4368–4386.

McPhaden, M. J., K. Ando, F. Syamsudin, G. Meyers, V. S. N. Murty, Y. Masumoto, M. Ravichandran, J. Vialard, L. Yu, and W. Yu (2008), RAMA: The research moored array for African-Asian-Australian monsoon analysis and prediction, *Bull. Am. Meteorol. Soc.*, in press.

Saji, N. H., S.-P. Xie, and C.-Y. Tam (2006), Satellite observations of intense intraseasonal cooling events in the tropical south Indian Ocean, *Geophys. Res. Lett.*, *33*, L14704, doi:10.1029/2006GL026525.

Shinoda, T., and H. H. Hendon (1998), Mixed layer modeling of intraseasonal variability in the tropical western Pacific and Indian oceans, *J. Clim.*, *11*, 2668–2685.

Sweeney, C., A. Gnanadesikan, S. M. Griffies, M. J. Harrison, A. J. Rosati, and B. L. Samuels (2005), Impacts of shortwave penetration depth on large-scale ocean circulation and heat transport, *J. Phys. Oceanogr.*, *35*, 1103–1119.

Vialard, J., et al. (2008), Air sea interactions in the Seychelles-Chagos thermocline ridge region, *Bull. Am. Meteorol. Soc.*, in press.

Wang, W., and M. J. McPhaden (1999), The surface layer heat balance in the equatorial Pacific Ocean. Part I: Mean seasonal cycle, *J. Phys. Oceanogr.*, *29*, 1812–1831.

Wentz, F. J., C. Gentemann, D. Smith, and D. Chelton (2000), Satellite measurements of sea-surface temperature through clouds, *Science*, *288*, 847–850.

Wheeler, M. C., and H. H. Hendon (2004), An all-season real-time multivariate MJO Index: Development of an index for monitoring and prediction, , *132*, 1917–1932.

Woolnough, S. J., F. Vitart, and M. A. Balmaseda (2007), The role of the ocean in the Madden-Julian Oscillation: Implications for MJO prediction, *Q. J. R. Meteorol. Soc.*, *133*, 117–128.

Zhang, C. (2005), Madden-Julian Oscillation, *Rev. Geophys.*, *43*, RG2003, doi:10.1029/2004RG000158.

C. de Boyer Montégut, Frontier Research Center for Global Change, JAMSTEC, Yokohama 236-0001, Japan.

J. P. Duvel, Laboratoire de Météorologie Dynamique, CNRS, F-75231 Paris CEDEX 05, France.

G. R. Foltz, Joint Institute for the Study of the Atmosphere and Ocean, University of Washington, Box 354925, Seattle, WA 98115, USA.

M. J. McPhaden, Pacific Marine Environment Laboratory, NOAA, 7600 Sand Point Way NE, Seattle, WA 98115, USA.

J. Vialard, LOCEAN – Case 100, Université Pierre et Marie Curie, F-75232 Paris CEDEX 05, France. (jv@locean-ipsl.upmc.fr)